Discovery of low-lying E1 and M1 strengths in ^{232}Th

A. S. Adekola, C. T. Angell, S. L. Hammond, A. Hill, C. R. Howell, H. J. Karwowski, J. H. Kelley, and E. Kwan

Phys. Rev. C **83**, 034615 — Published 25 March 2011

DOI: 10.1103/PhysRevC.83.034615

Discovery of low-lying $E1$ and $M1$ strengths in ^{232}Th

A. S. Adekola,[1,2,*] C. T. Angell,[3] S. L. Hammond,[1,2] A. Hill,[1,2]
C. R. Howell,[2,4] H. J. Karwowski,[1,2] J. H. Kelley,[2,5] and E. Kwan[2,4,†]

[1]*Department of Physics and Astronomy, University of North Carolina, Chapel Hill, North Carolina 27599 USA.*
[2]*Triangle Universities Nuclear Laboratory, Durham, North Carolina 27708 USA.*
[3]*Department of Nuclear Engineering, University of California, Berkeley, California, 94720 USA.*
[4]*Department of Physics, Duke University, Durham, North Carolina 27708 USA.*
[5]*Department of Physics, North Carolina State University, Raleigh, North Carolina 27695 USA.*

(Dated: February 28, 2011)

Properties of low-energy dipole states in ^{232}Th have been investigated with the nuclear resonance fluorescence technique. The present work used mono-energetic γ-ray beams at energies of 2 - 4 MeV from the high-intensity γ-ray source at Triangle Universities Nuclear Laboratory. Over 40 transitions corresponding to deexcitation to the ground state and first excited state were observed for the first time. Excitation energies, integrated cross sections, decay widths, branching ratios, and transition strengths for those states in ^{232}Th were determined and compared with quasi-particle random phase approximation calculations. Large number of $E1$ transitions were observed for the first time in actinide nuclei with summed strength of $3.28(69)\times10^{-3}e^2\text{fm}^2$. The observed summed $M1$ strength of 4.26(63) μ_N^2 is in good agreement with the other actinides and with the systematics of the scissors mode in deformed rare-earth nuclei.

PACS numbers: 23.20.Lv, 25.20.Dc, 27.90.+b

I. INTRODUCTION

Investigation of low-lying electric and magnetic dipole excitations in heavy-mass nuclei is of great importance to nuclear structure physics. There have been numerous experimental and theoretical efforts to study the orbital magnetic dipole response over a wide mass region [1–4]. Following the theoretical prediction [5] of low-lying collective $M1$ excitations known as the scissors mode in which the protons and neutrons in the nucleus undergo small angle vibrations in a scissors-like motion with respect to each other, it has been found experimentally in deformed nuclei using electron- and photon-scattering experiments [6, 7]. However, most of the investigations of $M1$ excitations have focused on light and on deformed rare-earth nuclei [4, 8] with limited experimental information on the actinides. Even less is known about $E1$ strength below the giant dipole resonance in the actinides. Unavailability of the polarized γ-ray beams until recently made unambiguous identification of $E1$ strength very difficult.

The study of scissors mode in the actinides is important because this region involves neutron-rich nuclei with large deformations. Previous measurements [9, 10] only accounted for scissors mode up to energies of 2.5 MeV for ^{232}Th and ^{238}U and 3.2 MeV for ^{236}U. Observed $M1$ excitations were concentrated in the energy region of 2 to 2.5 MeV with strengths comparable to those in mid-shell rare-earth nuclei [9]. Fragmentation of this strength in rare-earth nuclei is known to spread over an energy interval of 2.4 - 3.7 MeV with a mean energy of 3 MeV [8].

Theoretical calculations using quasi-particle random phase approximations (QRPA) predict the mean excitation energies, $\bar{E}_x$, as well as the summed $B(M1)$ and $B(E1)$ values in ^{232}Th, ^{236}U and ^{238}U [11, 12]. Consequently, it is desirable to obtain more experimental data on the distribution of the $M1$ and $E1$ strengths in actinides. It is expected that the $M1$ strength will gradually decrease with increasing excitation energy and the $E1$ strength will increase. However, γ spectroscopy of the ^{232}Th nucleus above 2.3 MeV is not known.

Nuclear resonance fluorescence (NRF) is an effective spectroscopic method to investigate collective $M1$ and $E1$ excitations in nuclei [13]. In this technique, interactions of a high-energy photon with a nucleus produce an excited state, which subsequently decays to lower-lying levels by emitting γ ray. This manuscript describes NRF measurements on a ^{232}Th target performed using nearly mono-energetic and 100% linearly-polarized γ-ray beams.

II. EXPERIMENT

The experiment was carried out at the High-Intensity γ-ray Source (HIγS) facility at the Triangle Universities Nuclear Laboratory (TUNL). Energetic photon beams at HIγS are created by Compton backscattering of a high-intensity free-electron laser (FEL) beam with an intense electron bunch. Comprehensive information about the operation and experimental capabilities of the facility is available in Ref. [14].

The present search for dipole excitations in ^{232}Th was performed at ten incident γ-ray beam energies between 2 and 4 MeV with average energy spread of FWHM = 5%. No data was taken at beam energy between 2.4 and 2.7 MeV due to the presence of a very strong background line

*Present address: Department of Physics and Astronomy, Rutgers University, Piscataway 08854 NJ USA.
†Present address: Physics Division, Lawrence Livermore National Laboratory, Livermore, California 94550, USA.

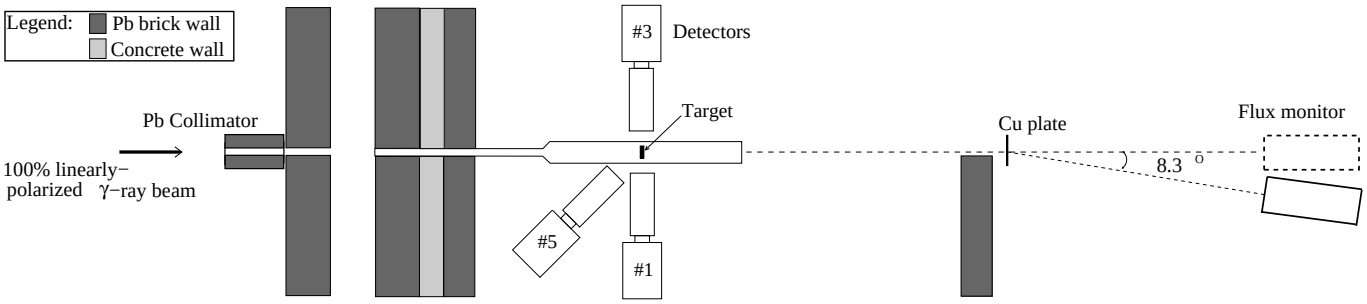

FIG. 1: Schematic diagram of the experimental layout showing two HPGe detectors at 90° and one at backward angle of 140° in the horizontal plane. The other two HPGe detectors in the vertical plane are not shown. The flux monitor at 0° (8.3°) is indicated as a dashed (solid) rectangle. Figure not drawn to scale.

at $E_\gamma = 2.614$ MeV. The energy distribution of the incident photons was measured using a large volume HPGe detector positioned into the beam. The photon flux was monitored by the same detector positioned at an angle of 8.3° relative to the beam axis. This detector measured Compton scattering of the γ-ray beam from a 1.1-mm thick copper plate positioned upstream perpendicular to the beam axis 167 cm away (see Fig. 1). The absolute flux was determined using the Klein-Nishina formula [15] from the spectrum of the Compton-scattered photons, corrected for the detector response with error no greater than 7%. The Compton scattering technique was verified against known resonance strength in ^{11}B [16].

The photon beams passed through a 30.5-cm long lead collimator with a cylindrical hole of 2.22 cm in diameter, located at about 52.5 m from the collision point of the electrons with the FEL photons. The collimator ensures that the beam, illuminating a 0.1-cm thick ^{232}Th foil, was smaller than the surface area of the target, inclined at 61.4° relative to the incident beam. The target was enriched to 99.9%.

A schematic drawing of the experimental setup is shown in Fig. 1. The NRF γ rays from the target were measured with a HPGe detector array positioned about 4.8 m downstream from the collimator. The array consists of four HPGe detectors with 60% efficiency relative to a 7.62 cm × 7.62 cm NaI scintillation detector. These detectors were positioned 10 cm away from the center of the target and 90° relative to the beam. Two of these detectors were located in the horizontal plane (called horizontal detectors) and the other two in the vertical plane (called vertical detectors). An additional HPGe detector was placed in the horizontal plane at backward angle of 140°. This detector configuration allows for unambiguous determination of multipolarities of observed γ-ray transitions. The uncertainty of the detectors geometry was estimated to be 4%. Part of the data were taken without one of the horizontal detectors. The detectors had passive shielding and absorbers composed of Pb and Cu. This helped to reduce the contributions from low-energy background.

The energy calibrations came from the known decay lines of ^{232}Th and a radioactive ^{60}Co source. The detector efficiencies $\epsilon(E_\gamma)$ were obtained by combination of calibrated radioactive ^{60}Co and ^{56}Co source measurements with error no greater than 4%. GEANT4 simulations were used to extrapolate $\epsilon(E_\gamma)$ to the energies above 3.6 MeV. The effects of atomic absorption of γ rays in the target were also accounted for in the simulations.

The signals from the detectors were processed by individual multi-channel analyzers with 14-bit analog-to-digital converters allowing the spectra to be binned to 0.27 keV/channel. The dead time of the the acquisition system was estimated from comparison of the 1.33 MeV peak area of a ^{60}Co source located near the HPGe array, with and without beam.

III. ANALYSIS AND CALCULATION

The integrated NRF cross section I_s at deexcitation energy E_γ is given by:

$$I_s = \frac{2J_x+1}{2J_0+1}\left(\frac{\pi\hbar c}{E_\gamma}\right)^2 \Gamma_0 \frac{\Gamma_f}{\Gamma}, \qquad (1)$$

where J_0 and J_x are the spins of the ground and the excited states, respectively, Γ_f is the decay width to the final state, Γ_0 and Γ are the ground-state decay width and total width, respectively, and Γ_f/Γ is the branching ratio. In the present measurement, only deexcitations to the ground state and the first excited state of 49 keV with $J^\pi = 2^+$ have been observed. Consequently, the branching ratio becomes Γ_1/Γ and $\Gamma = \Gamma_0 + \Gamma_1$, where Γ_1 is the decay width to the first excited state. From the experimental observables, I_s can be deduced from

$$I_s = \frac{N}{n_t \epsilon(E_\gamma) W(\theta,\phi)\Phi}, \qquad (2)$$

where N is the number of counts in the peak, n_t is the number of target nuclei per unit area, and Φ is the number of incident γ rays. The factor $W(\theta,\phi)$ describes the angular distribution where θ is the polar angle of the outgoing radiation with respect to the linearly-polarized

beam and ϕ is the azimuthal angle measured from the polarization plane.

In the NRF technique, a photon beam incident on a nucleus selectively populates dipole states with the highest probability. The measurement of the angular distribution of deexcitation photons γ_2 with respect to the incoming linearly-polarized photon beam γ_1 via the sequence $J_0 \stackrel{\gamma_1}{\rightarrow} J_x \stackrel{\gamma_2}{\rightarrow} J_0$ allows a spin assignment of the excited state in the even-even nuclei. The angular correlations calculated for the most probable spin sequences relevant to the present work are presented in Table I. The use of linearly-polarized photons makes it possible to determine parity assignment of the excited states from the measured azimuthal asymmetry. The asymmetry has maximal values of -1 (+1) for $E1$ ($M1$) transition (for a point-like detector).

For even-even nuclei, the reduced transition probabilities are related to the measured Γ_0 by:

$$B(E1) = 2.87 \times 10^{-3} \frac{\Gamma_0}{E_\gamma^3} \quad [e^2\mathrm{fm}^2], \tag{3}$$

and

$$B(M1) = 0.26 \frac{\Gamma_0}{E_\gamma^3} \quad [\mu_N^2], \tag{4}$$

where E_γ is in MeV and Γ_0 is in meV.

In the deexcitation of most of the states observed in this work branching to the first excited level (J^π=2^+) was identified. The branching ratio is given by:

$$R_{exp} = \frac{B(J = 1^\pm \rightarrow 2^+)}{B(J = 1^\pm \rightarrow 0^+)} = \frac{\Gamma_1}{\Gamma_0} . \frac{E_{\gamma 0}^3}{E_{\gamma 2}^3}, \tag{5}$$

where E_{γ_0} and E_{γ_2} are the transition energies to the ground-state and to the 2^+ state, respectively.

IV. RESULTS AND DISCUSSION

The spectra collected at beam energy of 2.9 MeV are shown in Fig. 2 revealing the $M1$ transitions observed at this energy. The spectrum of the observed γ rays with the two vertical and horizontal detectors added together are shown in the upper and middle panels, respectively, while the third spectrum in this figure shows the spectrum of γ rays observed in the detector located at backward angle of 140°. Similar spectra collected at beam energy of 3.6 MeV are shown in Fig. 3 revealing the $E1$ transitions observed at this energy. The spectrum of the observed γ rays with one horizontal and average of two vertical detectors are shown in the upper and bottom panel, respectively. The transitions appearing in the horizontal (vertical) but not in the vertical (horizontal) detectors correspond to pure $M1$ ($E1$) excitations.

In the spectra shown in Fig. 2, the peak at 2885.8 keV

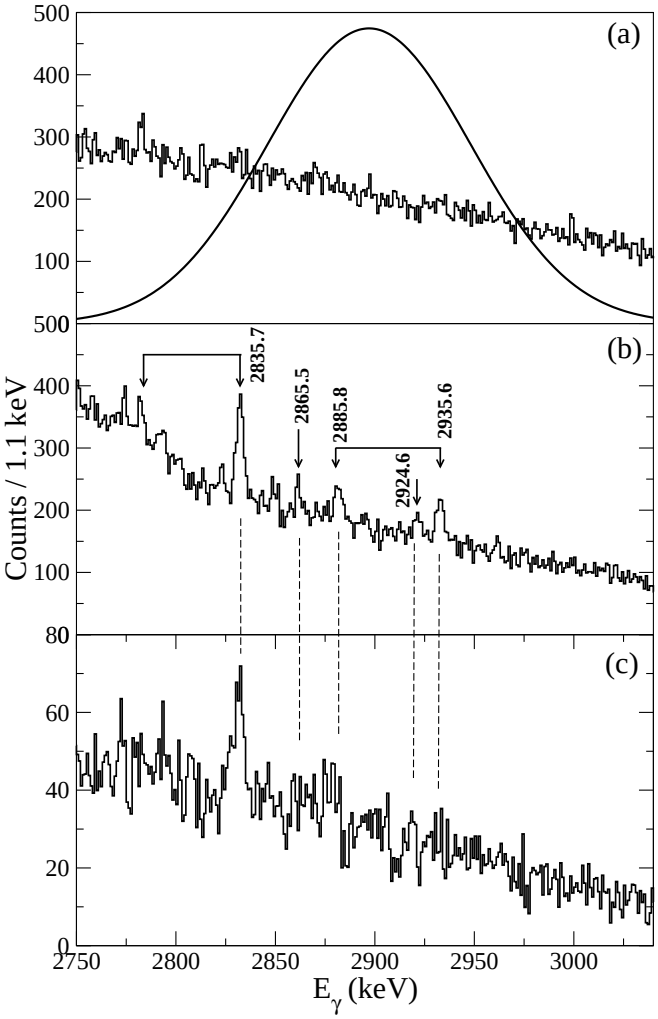

FIG. 2: The spectra from the ^{232}Th($\vec{\gamma}, \gamma'$) reaction at photon energy of 2.9 MeV in the two vertical detectors (a), two horizontal detectors (b) and in the backward angle detector (c). The line in (a) shows the energy distribution of the photon flux, Φ in arbitrary unit. The brackets in (b) connect the ground state transitions from the $J^\pi = 1^+$ levels with their corresponding transitions to the 2^+ state, separated by 49 keV while the single arrows are ground state transitions without detectable branching to the 2^+ state. The ground state transition at 2885.8 keV coincides with the branching from the 2935.6 keV level. The same is true for ground state transition at 2835.7 keV and the branching transition from the 2885.8 keV state.

TABLE I: Angular correlations in the detector array.

		Horizontal	Vertical	Backward
$M1$	$0^+ \stackrel{\gamma_1}{\rightarrow} 1^+ \stackrel{\gamma_2}{\rightarrow} 0^+$	1.45	0.08	1.5
	$0^+ \stackrel{\gamma_1}{\rightarrow} 1^+ \stackrel{\gamma_2}{\rightarrow} 2^+$	1.1	0.9	1.05
$E1$	$0^+ \stackrel{\gamma_1}{\rightarrow} 1^- \stackrel{\gamma_2}{\rightarrow} 0^+$	0.09	1.45	0.88
	$0^+ \stackrel{\gamma_1}{\rightarrow} 1^- \stackrel{\gamma_2}{\rightarrow} 2^+$	0.9	1.1	0.96
$E2$	$0^+ \stackrel{\gamma_1}{\rightarrow} 2^+ \stackrel{\gamma_2}{\rightarrow} 0^+$	2.5	0	1.47
	$0^+ \stackrel{\gamma_1}{\rightarrow} 2^- \stackrel{\gamma_2}{\rightarrow} 0^+$	0	2.5	0.08

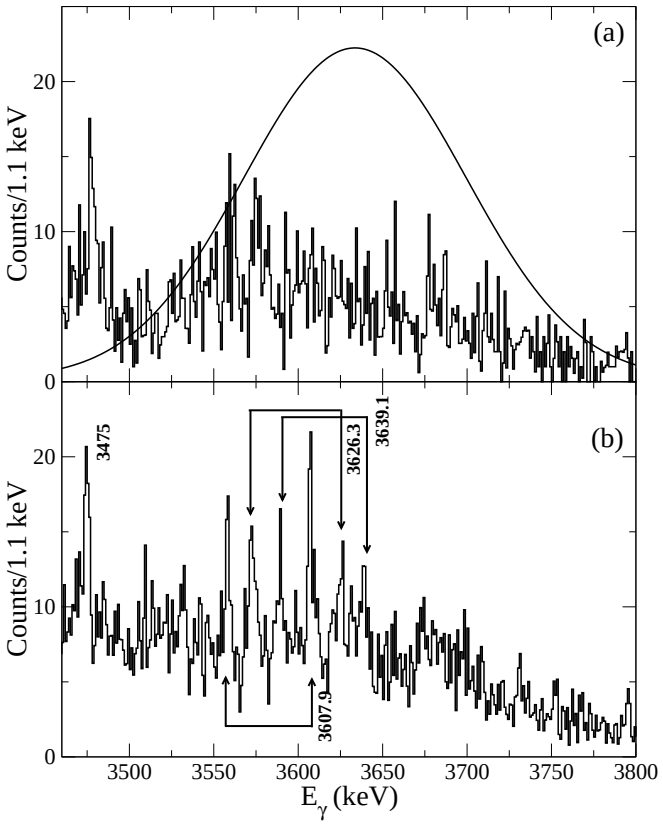

FIG. 3: The spectra from the ^{232}Th$(\vec{\gamma},\gamma')$ reaction at photon energy of 3.6 MeV in the horizontal (a) and vertical detectors (b). The line in (a) shows the energy distribution of the photon flux, Φ in arbitrary unit. The brackets in (b) connect the ground state transitions from the $J^\pi = 1^-$ levels with their corresponding transitions to the 2^+ state, separated by 49 keV. The peak at 3475 keV is a background line due to the activity in the target.

is expected to be of equal intensity in all the detectors after correcting for efficiency, if it is truly the branching of the 2935.6 keV state. However, this was not what was observed; rather the peak was more intense in the horizontal than vertical detectors. A $M1$ ground-state transition coinciding with the branching transition exists, which gives more intensity in the horizontal detectors. The intensity of this $M1$ transition was obtained by subtracting the intensity of the branching in the horizontal detectors based on the intensity of the branching in the vertical detectors. The data was analyzed in this fashion in order to set an upper limit on the branching ratio for the 2935.6 keV state. The same procedure was adopted in extracting the intensity of the $M1$ ground state at E$_\gamma$ = 2835.7 keV, which coincides with the branching of the 2885.8-keV state.

A total of 21 states were identified which decay to the ground state as well as to the 2^+ state. The branching transitions to the 2^+ state were identified from the 49-keV energy differences of the observed peaks. Five levels were observed without detectable branching to the 2^+ state. However, an upper limit on the branching ratio has been determined for each of these five levels. The level energies deduced for all the states, the integrated cross sections, the branching ratios, the decay widths to the ground state, and the strengths determined for all the transitions are presented in Table II. Most of the observed transitions reported in Table II were above the 3σ detection limit P defined as [17]

$$P = 3.3\sqrt{2S}, \tag{6}$$

where S is the integral over the background with length of 3σ, and σ is the dispersion of a Gaussian fit of the peaks observed at the same energy. The transitions observed with 2σ detection limit are also included in Table II. The detection limits were converted to minimal detectable I_s using Eq. 2. The area S is calculated from the background spectrum using the dependence of FWHM on the γ-ray energy obtained from the calibrated radioactive source measurements. As an example, a comparison of the minimal detectable I_s at incident beam energy of 2.9 MeV and the measured integrated cross-sections is shown in Fig. 4.

In Fig. 5, the strength distributions of the $M1$ and $E1$ excitations observed in this work are presented along with previous experimental data from Heil *et al.* [9]. The errors on the $M1$ and $E1$ strengths reported in Table II and Fig. 5 are statistical only. The sources of systematic errors in the observed strength are listed in Table III. The overall systematic error of 9% was obtained by adding in quadrature all contributing errors. Systematic error on the energy is estimated to be 0.5 keV. For the previously known dipole excitations below 2.5 MeV, the $M1$ strengths of 1.34(13), 0.79(9) and 0.39(4) μ_N^2 were determined for the states observed at E_x = 2.043, 2.249 and 2.296 MeV, respectively. These values agree well with $M1$ strengths of 1.48(9), 0.56(7) and 0.31(6) μ_N^2, respectively reported in Ref. [9]. This comparison also serves as a test to the overall procedure in our data

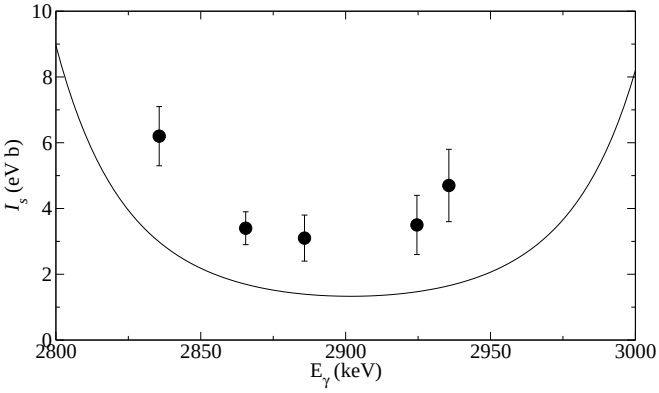

FIG. 4: Detection limit P normalized to cross section I_s as a function of γ-ray energy at nominal beam energy of 2.90 MeV. For comparison, experimentally determined I_s values are shown.

TABLE II: Excited states observed in the the NRF experiment on ^{232}Th. Except where indicated, the detection limit of 3σ confidence level was used.

	E_x (keV)	I_s (eV b)	R_{exp}	Γ_0^2/Γ (meV)	$B(M1)$ (μ_N^2)
1	2043.7(3)[a]	46.3(45)	0.62(9)	16.8(16)	1.34(13)
2	2249.5(5)[a,b]	25.5(28)	0.48(8)	11.2(12)	0.79(9)
3	2296.3(6)[a]	19.0(18)	0.89(12)	8.7(8)	0.39(4)
4	2795.2(4)	4.4(8)	0.71(21)	3.0(5)	0.08(2)
5	2835.0(3)	6.2(9)	0.78(17)	4.3(6)	0.15(2)
6	2865.5(7)	3.4(5)	<0.19(5)	2.4(4)	0.17(3)
7	2885.8(4)	3.1(7)	<0.26(5)	2.2(5)	0.12(3)
8	2924.6(5)	3.5(9)	<0.11(3)	2.6(6)	0.27(7)
9	2935.6(3)	4.7(11)	0.44(9)	3.5(8)	0.12(3)
10	2996.3(9)[b]	2.3(6)	1.37(50)	1.8(5)	0.03(1)
11	3014.4(7)	3.0(7)	<0.17(6)	2.4(5)	0.16(4)
13	3115.1(5)	7.7(15)	<0.10(3)	6.5(13)	0.61(12)
14	3287.1(6)	1.9(4)	0.80(24)	1.8(3)	0.03(1)
	E_x (keV)	I_s (eV b)	R_{exp}	Γ_0^2/Γ (meV)	$B(E1)$ ($10^{-3}e^2$fm^2)
1	3060.4(7)	2.1(4)	0.73(20)	1.7(3)	0.40(7)
2	3395.8(8)[b]	0.9(2)	0.96(34)	0.9(2)	0.13(3)
3	3607.9(9)	2.2(6)	0.74(18)	2.5(7)	0.36(10)
4	3626.3(3)	1.9(3)	1.07(23)	2.1(4)	0.25(4)
5	3639.1(6)	1.1(2)	1.29(32)	1.3(2)	0.14(3)
6	3731.5(8)	2.0(4)	0.61(16)	2.4(4)	0.34(6)
7	3742.6(2)	1.6(3)	0.75(23)	2.0(4)	0.26(5)
8	3752.4(7)[b]	1.3(3)	1.05(36)	1.6(4)	0.17(4)
9	3820.7(2)	1.5(3)	0.40(14)	1.8(3)	0.33(6)
10	3920.8(6)	1.6(3)	0.47(13)	2.1(3)	0.32(5)
11	3935.8(8)	1.1(2)	0.74(23)	1.4(3)	0.16(3)
12	4002.2(6)[b]	3.0(8)	0.76(32)	4.2(11)	0.44(12)

[a] Previously observed by Heil *et al.* [9].
[b] 2σ confidence limit.

analysis. All the states above 2.5 MeV listed in Table II were observed for the first time. No $E2$ transitions were observed within 2σ detection limit.

Theoretical calculations of low-lying electric 1^- and magnetic 1^+ dipole states in ^{232}Th, within the quasi-particle random-phase approximation (QRPA) approach [12] are shown as solid lines in Fig. 5. This QRPA calculation provides a simultaneous description of 1^+ and 1^- states after the restoration of rotational, translational, and Galilean invariance by separable forces. It was used successfully in the past to describe dipole excitations in rare-earth nuclei [3] and permitted a direct comparison with NRF data.

TABLE III: Systematic error budget for the observed strengths.

Sources of error	Value %
Detectors array efficiency	3
Detectors geometry	4
Target thickness	3
Beam flux	7
Total uncertainty	9

The concentration of $M1$ dipole states clustered around 2.8 MeV consists of most of the newly observed $M1$ excitations each with relatively small strength. A calculation of orbit-to-spin ratio for actinides using QRPA with a deformed Woods-Saxon potential and separable residual interactions was performed by Nojarov *et al.* [11]. In this energy region, the calculated orbit-to-spin ratio for actinides shows that the 1^+ excitations have large orbital contribution to the $M1$ transition matrix element. For this reason, we are assuming scissors mode for all the newly observed $M1$ transitions. The $M1$ strength gradually decreases with increasing excitation energy as expected.

Systematics of the variation of observed summed $B(M1)$ strength with deformation was investigated for even-even rare-earth nuclei in Ref. [1]. The quantity

$$\xi = \sum B(M1)(\mu_N^2)A^{2/3}Z^{-2}, \tag{7}$$

was found to depend linearly on the square of the deformation δ as

$$\xi \approx 0.27\delta^2. \tag{8}$$

For ^{232}Th using $\delta = 0.216$, Eq. 8 gives $\xi = 0.013$ which is close to the experimentally determined $\xi = 0.02(3)$ using Eq. 7.

The distributions of $M1$ and $E1$ strengths calculated in Ref. [12] seem to follow a similar pattern with substantial $E1$ strength predicted between 3.3 and 3.8 MeV. The

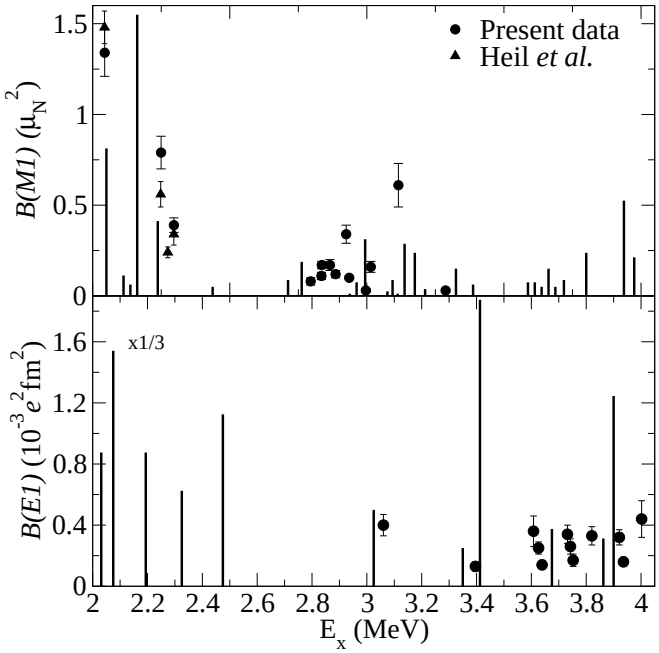

FIG. 5: Comparison of experimental and calculated $B(M1)$ (upper panel) and $B(E1)$ (lower panel) in ^{232}Th. The solid line in both panels represents QRPA calculated values [12]. The calculated $E1$ transition at 2.1 MeV has been scaled down by a factor of 3.

TABLE IV: Comparison of experimental and calculated $B(M1)$ strength in actinides.

	Experiment					Theory					
Target	^{232}Th^a	^{232}Th^b	^{235}U^c	^{236}U^d	^{238}U^b	^{232}Th^e	^{236}U^e	^{238}U^e	^{232}Th^f	^{236}U^f	^{238}U^f
Energy range (MeV)	$2-4$	$1.9-2.4$	$2.2-2.8$	$1.8-3.2$	$2-2.6$	$2-3$			$2-4$		
$\bar{E}_x$ (MeV)	2.5(4)	2.1(2)	2.5(3)	2.2(2)	2.3(2)	2.5	2.6	2.6	2.6	2.6	2.7
$\sum B(M1)(\mu_N^2)$	4.3(6)	2.6(3)	3.6(13)	2.9(2)	3.2(2)	2.7(5)	5.4(17)	5.0(8)	5.0	6.1	5.7

^{a}Present work, ^{b}Ref. [9], ^{c}Ref. [18], ^{d}Ref. [10], ^{e}Ref. [8], ^{f}Ref. [12].

summed $M1$ transition strength in ^{232}Th calculated from the present data is 4.26(63) μ_N^2 with $\bar{E}_x = 2.49(37)$ MeV which was determined using

$$\bar{E}_x = \frac{\sum_i E_{xi} B(M1)_i}{\sum_i B(M1)_i}. \quad (9)$$

The contribution of the newly found $M1$ transitions is about 40% of the total observed strength. The mean excitation energy is in agreement with $\bar{E}_x = 2.32$ MeV calculated using $\bar{E}_x \approx 66\delta A^{-1/3}$ for scissors mode, where δ is the deformation parameter and A is the mass number [1, 6]. This formula successfully described the variation of strength with deformation in a wide range of rare-earth nuclei. This observed $M1$ strength is presented in Table IV and the value is similar to the strengths of the scissors mode in ^{236,238}U [9, 10].

The predictions of the centroid of the scissors mode excitation energy in ^{232}Th and ^{236,238}U and their expected summed strengths using the sum-rule approach [8] and using QRPA calculation [12] are also shown in Table IV. The QRPA calculation predicts strength at energy above 3.3 MeV which is not experimentally observed. Thus, it overestimates the summed $M1$ strength and the sum-rule prediction underestimates the summed $M1$ strength.

We observe a fragmentation of the $M1$ strengths spread from 2.0 to 3.3 MeV. It is consistent with the general trend of QRPA calculations, which predict $M1$ strengths distributed among 22 1^+ states with 16 of the predicted transitions having strength $\lesssim 0.15$ μ_N^2. However, there are some differences between the data and the details of the calculations that can be most likely attributed to the fragmentation of the strength into transitions that are below the present detection limit. The spreading of $M1$ strength observed for ^{232}Th is similar to that in the other actinides [9, 10] and in the rare-earth nuclei [19, 20].

The summed $E1$ transition strength of $3.28(69)\times10^{-3}e^2\mathrm{fm}^2$ is contained in twelve newly observed states with $\bar{E}_x$=3.69(77) MeV. A considerable $E1$ strength is predicted in the energy range from 2 to 2.5 MeV which is not experimentally observed. In this measurement, the $E1$ transitions start to appear at about $E_x = 3$ MeV with some gradual increase in the concentration of the observed states with increasing excitation energy. This increase may arise from the tail of the giant dipole resonance or may represent the so-called pygmy $E1$ resonance observed previously in a wide range of nuclei. It is the first time $E1$ transitions were clearly observed in actinide nuclei.

In summary, NRF experiments on ^{232}Th have been performed at the HIγS facility using 100% linearly-polarized and nearly mono-energetic beams with energies from 2 to 4 MeV. High quality beams allowed observation of more than 20 discrete deexcitations to the ground state and the branching transitions to the first excited state were identified for most of them. Considerable $E1$ strength was identified at excitation energies between 3 and 4 MeV. Twelve $E1$ and ten $M1$ excitations are observed in this work for the first time. The observed $M1$ strength is in agreement with other actinides and the systematics of the scissors mode observed in even-even rare-earth nuclei.

ACKNOWLEDGMENTS

We acknowledge with thanks, the staff of the HIγS facility at Triangle University Nuclear Laboratory for their technical support in making this experiment possible. We thank E. B. Norman of University of California, Berkeley for loaning us the ^{232}Th target, D. Ticehurst, J. Tompkins, R. Raut, G. Rusev, W. Tornow and A. P. Tonchev for help in data taking and helpful discussions. We thank Dr. E. Guliyev for sharing the results of his calculations. This work was supported in part by the U.S. Department of Homeland Security grant numbers 2008-DN-077-ARI010, 2008-DN-077-ARI014 and Department of Energy grant numbers DE-FG52-06NA26155, DE-FG02-97ER41033 and DE-FG02-97ER41042. The author, ASA acknowledges the support by the National Nuclear Security Administration under the Stewardship Science Academic Alliances program through U.S. Department of Energy Cooperative Agreement DE- FG52-08NA28552 and the National Science Foundation.

[1] N. Pietralla *et al.*, Phys. Rev. C **58**, 184 (1998).

[2] A. Richter, Prog. Part. Nucl. Phys. **34**, 261 (1995).

[3] F. Ertugral, E. Guliyev, A. Kuliev, and Z. Yildirim, Cent. Eur. J. Phys **7**, 731 (2009).
[4] K. Heyde et al., Rev. Mod. Phys. (accepted) (2010).
[5] F. Iachello, Phys. Rev. Lett. **53**, 1427 (1984).
[6] U. Kneissl, H. H. Pitz, and A. Zilges, Prog. Part. Nucl. Phys. **37**, 349 (1996).
[7] H. Maser *et al.*, Phys. Rev. C **54**, R2129 (1996).
[8] J. Enders *et al.*, Phys. Rev. C **71**, 014306 (2005).
[9] R. D. Heil *et al.*, Nucl. Phys. **A476**, 39 (1988).
[10] J. Margraf *et al.*, Phys. Rev. C **42**, 771 (2000).
[11] R. Nojarov *et al.*, Nucl. Phys. **A563**, 349 (1993).
[12] A. A. Kuliev, E. Guliyev, F. Ertugral1, and S. Özkan, Eur. Phys. J. A **43**, 313 (2010).
[13] E. P. U. Berg and U. Kneissl, Ann. Rev. Nucl. Part. Sci. **37**, 33 (1987).
[14] H. R. Weller *et al.*, Prog. Part. Nucl. Phys. **62**, 257 (2009).
[15] G. F. Knoll, Radiation Detection and Measurement (John Wiley and Sons, Inc.,2000).
[16] G. Rusev, A. P. Tonchev, R. Schwengner, C. Sun, W. Tornow, and Y. K. Wu, Phys. Rev. C **79**, 047601 (2009).
[17] D. A. Gedcke, ORTEC Application Note AN59 (2005).
[18] O. Yevetska *et al.*, Phys. Rev. C **81**, 044309 (2010).
[19] H. Friedrichs *et al.*, Nucl. Phys. **A567**, 266 (1994).
[20] H. H. Pitz *et al.*, Nucl. Phys. **A492**, 411 (1989).